

1  
2  
3  
4  
5  
6  
7  
8  
9  
10  
11  
12  
13  
14  
15  
16  
17  
18  
19  
20

*Geophysical Research Letters*

Supporting Information for

**Evaluating Uncertainty and Modes of Variability for Antarctic Atmospheric Rivers**

**Christine A. Shields<sup>1</sup>, Jonathan D. Wille<sup>2</sup>, Allison B. Marquardt Collow<sup>3,4</sup>, Michelle  
Maclennan<sup>5</sup>, Irina V. Gorodetskaya<sup>6</sup>**

<sup>1</sup>National Center for Atmospheric Research, Climate and Global Dynamics Laboratory, Boulder,  
Colorado

<sup>2</sup>Institut des Géosciences de l'Environnement, CNRS/UGA/IRD/G-INP, Saint Martin d'Hères,  
France

<sup>3</sup>University of Maryland Baltimore County, Baltimore, MD

<sup>4</sup>Global Modeling and Assimilation Office, NASA Goddard Space Flight Center, Greenbelt, MD

<sup>5</sup>University of Colorado, Department of Atmospheric and Oceanic Science, Boulder, Colorado

<sup>6</sup>CESAM – Centre for Environmental and Marine Studies, Department of Physics, University of  
Aveiro, Aveiro, Portugal

Corresponding author: Christine A. Shields (shields@ucar.edu)

21 **Contents of this file**

22

23 Text S1

24 Text S2

25 Figures S1 to S4

26 Tables S1

27

28 **Introduction**

29 Details for Antarctic-specific Wille ARDTs and computation of MOVs are provided as text. An  
 30 Antarctic regional map, ARTMIP climatology frequency and seasonal cycle metrics for both  
 31 Tier 1 and Tier 2 ARTMIP projects are provided as figures. ARTMIP ARDTs included in this  
 32 study, with associated references and DOIs are provided in table format. Basic state figures for  
 33 MOVs are provided for both spatial pattern and timeseries.

34

35 **Text S1.**

36

37 Standard IVT and IWV calculation

38 Traditional ARDTs designed for the mid-latitudes typically apply moisture thresholds using the  
 39 quantity called integrated vapor transport (IVT), calculated as Eq. (1), which combines specific  
 40 humidity with both zonal ( $u$ ) and meridional ( $v$ ) as such:

$$41 \quad (1) \text{ IVT} = -\frac{1}{g} \int_{Pb}^{Pt} (q \mathbf{V}h) dp$$

42

43 where  $q$  is the specific humidity,  $\mathbf{V}_h$  is the horizontal wind vector,  $P_b$  is pressure at the bottom of the  
 44 atmosphere, typically 1000 hPa,  $P_t$  is at the top of the atmosphere, typically 200hPa, and  $g$  is the  
 45 acceleration due to gravity.

46

47 Identification based solely on moisture stream, or integrated water vapor (IWV) (Eq. 2) is also  
 48 commonly used and is expressed as Eq. (2):

49

$$50 \quad (2) \text{ IWV} = -\frac{1}{g} \int_{Pb}^{Pt} q dp$$

51

52 which integrates the total column water without any wind information (Shields et al., 2018).

53

54

55

56 Antarctic AR Detection Tool, Wille  $v$ IVT and Wille IWV

57 Moisture thresholds for the Wille “ $v$ IVT” ARDT, use anomalies of the *meridional* component to  
 58 the integrated water vapor ( $v$ IVT) expressed as

$$vIVT = -\frac{1}{g} \int_{surface}^{top} (q v_h) dp$$

where  $v_h$  is the meridional component of the wind,  $q$  is the specific humidity,  $p$  atmospheric pressure (hPa), and  $g$  is the acceleration due to gravity. Full reanalysis levels are used.

The Wille “IWV” ARDT algorithm uses integrated water vapor anomalies similar to the traditional method with the exception of using full reanalysis model levels. It can be expressed as

$$IWV = -\frac{1}{g} \int_{surface}^{top} q dp$$

where  $q$  is the specific humidity,  $p$  atmospheric pressure (hPa), and  $g$  is the acceleration due to gravity.

Both Wille\_vIVT and Wille\_IWV compute moisture thresholds defined as the 98th percentile in mean monthly climatological IWV or vIVT for all grid cells calculated using reanalysis data. Geometry requirements focus on the latitudinal footprint. Shapes are tested for a minimum continuous 20° latitude span between 37.5° S - 80.0° S. More details and application can be found in Wille et al. 2019 and Wille et al. 2021.

#### ARTMIP ARDTs

A summary of all over ARDTs is found in Table S1.

## **Text S2.**

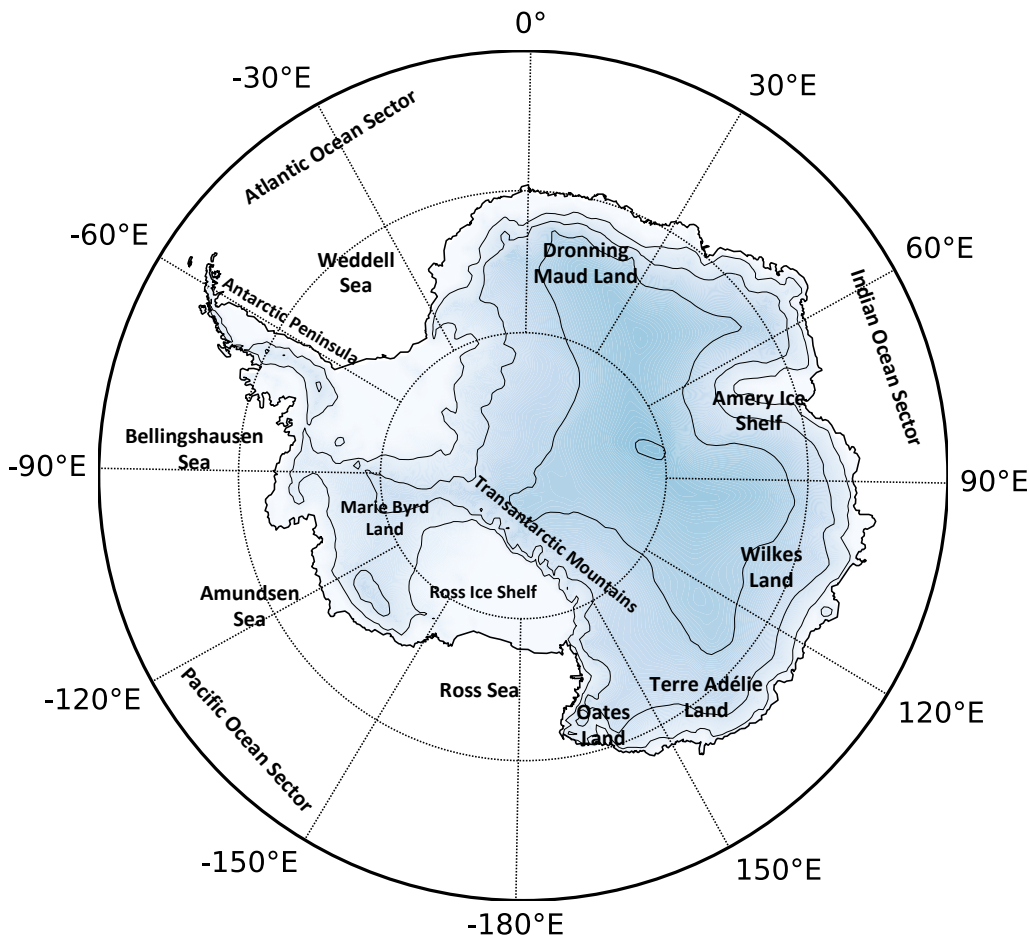
### Decadal Modes of Variability

Decadal modes include both the Southern Annular Mode (SAM) and the Pacific Decadal Oscillation (PDO). SAM is calculated classically as the leading EOF of the detrended 500 hPa geopotential anomalies for the southern hemisphere from 20°S to 90°S. Principle component (PC) time series are regressed onto precipitation and 850 hPa temperature for AR days to show correlation of AR characteristics with SAM. PDO is defined as the leading principal component of the North Pacific Ocean (20:70°N, 110°E:100°W) of the detrended sea surface temperature anomalies. Spatial patterns and PC timeseries for both SAM and PDO are shown in Supplemental Figure S2.

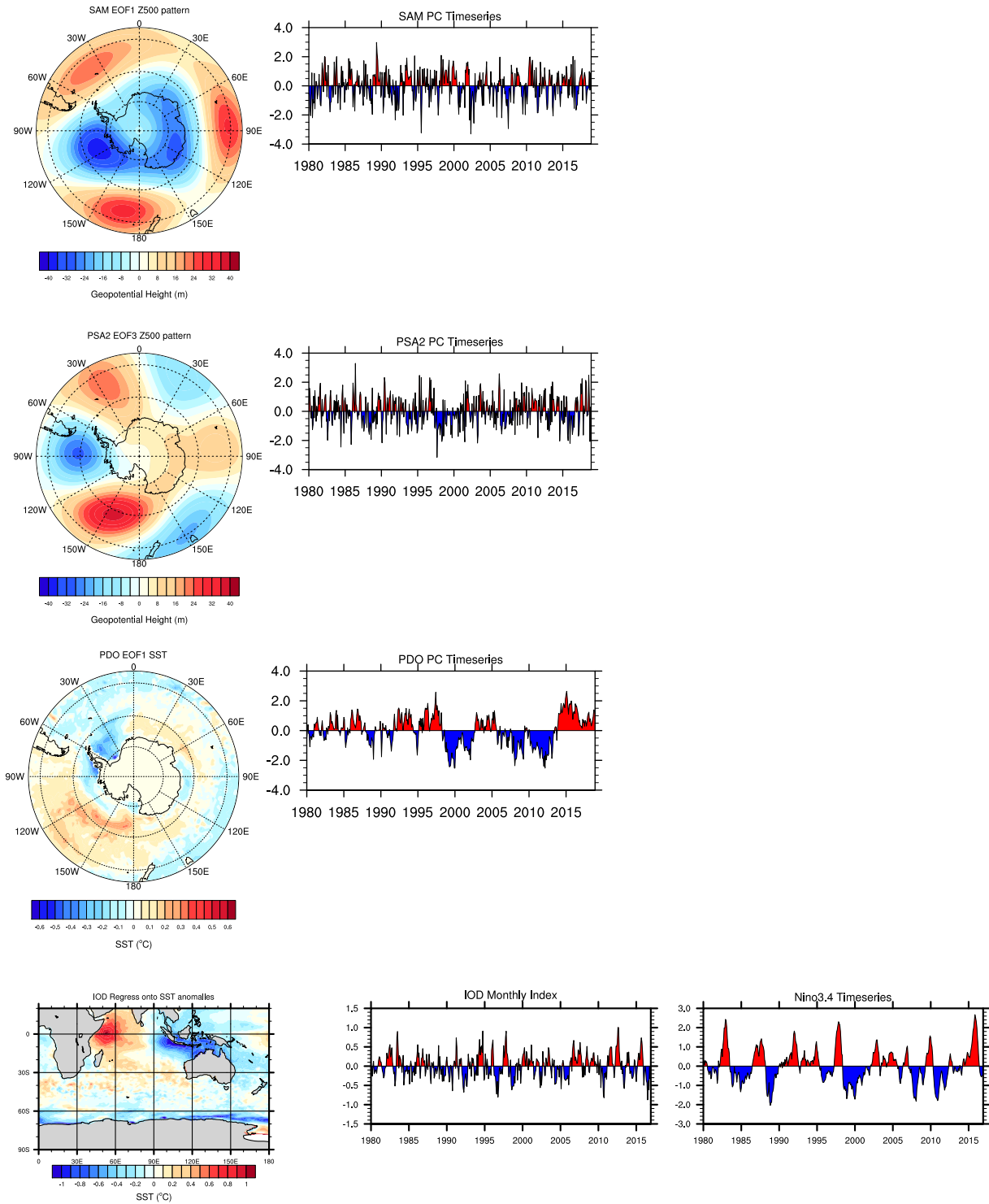
### Interannual Modes of Variability

Interannual modes include the 2nd Pacific South American pattern, (PSA2), and the Indian Ocean Dipole (IOD), both in and out of phase with El Niño Southern Oscillation (ENSO). The first pattern of PSA (PSA1) is not shown because it lacks significance with AR days. PSA2 is defined as the 3rd EOF of detrended 500 hPa geopotential height anomalies, which is the same domain and approach as SAM. Not only does EOF3 of 500 hPa geopotential height have implications for Antarctic ARs, it has also been shown as important for extratropical moisture transport, especially for western North America (O’Brien et al, 2022 in revision). The IOD is

103 calculated by differencing detrended, area-averaged sea surface temperature anomalies between  
 104 10°S-10°N and 50-70°E versus 0-10°S and 90-110°E. For ENSO, we choose to apply the  
 105 combined Niño3.4 region to emphasize more centralized equatorial sea surface temperatures.  
 106 Area-averaged SST anomalies for Niño3.4 are computed over 5°S-5°N and 120-170°W. For  
 107 MOV analysis, the IOD index, both in and out of phase with ENSO, is regressed onto  
 108 precipitation and 850 hPa temperatures for AR days. PSA2 and IOD patterns and timeseries are  
 109 shown in Supplemental Figure S2.  
 110  
 111  
 112  
 113

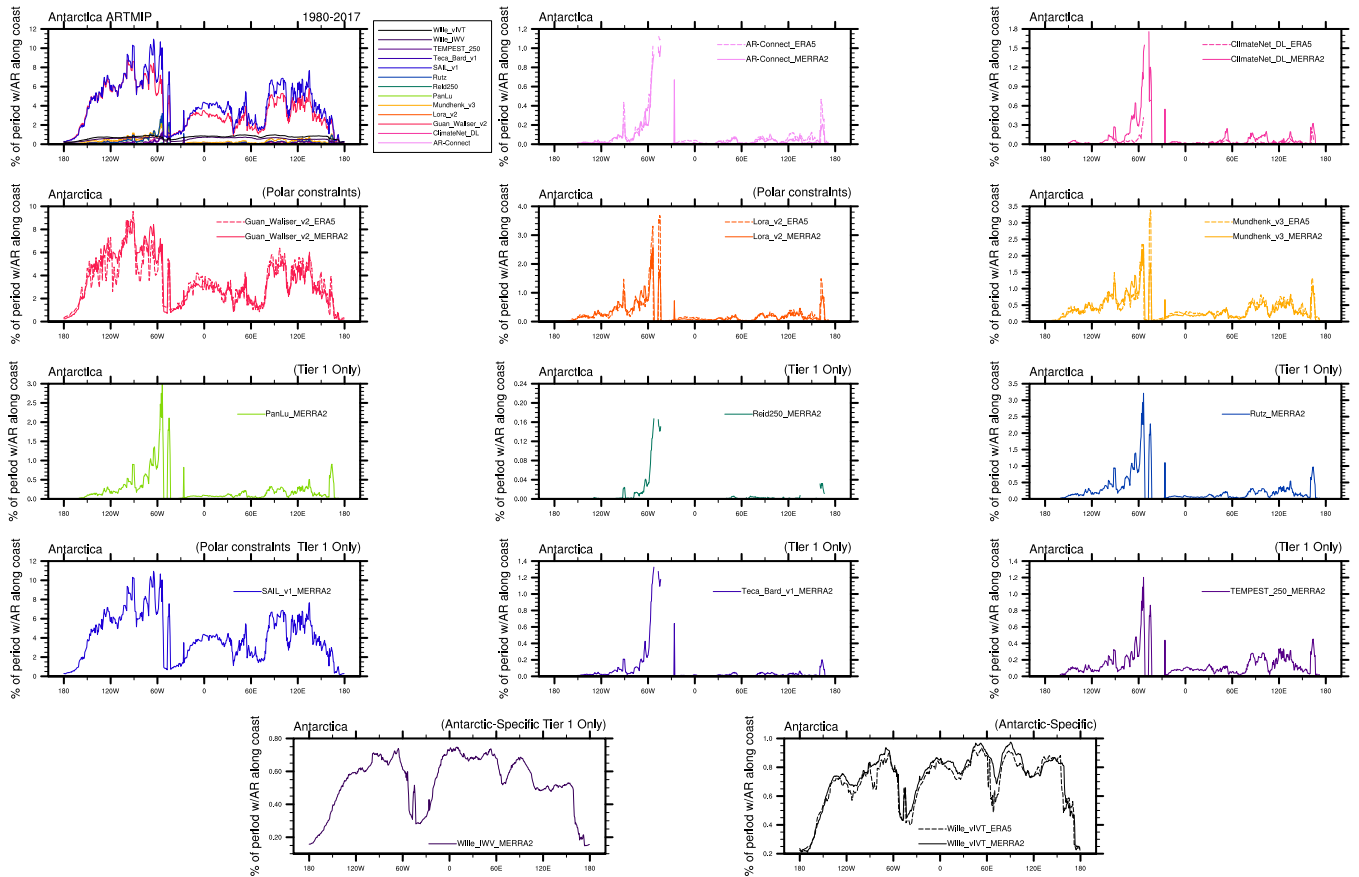


114  
 115 **Figure S1.** Antarctic map with labels identifying regions discussed in the main article. Blue  
 116 shading and contours represent topography.  
 117  
 118  
 119



120  
121  
122  
123  
124  
125  
126

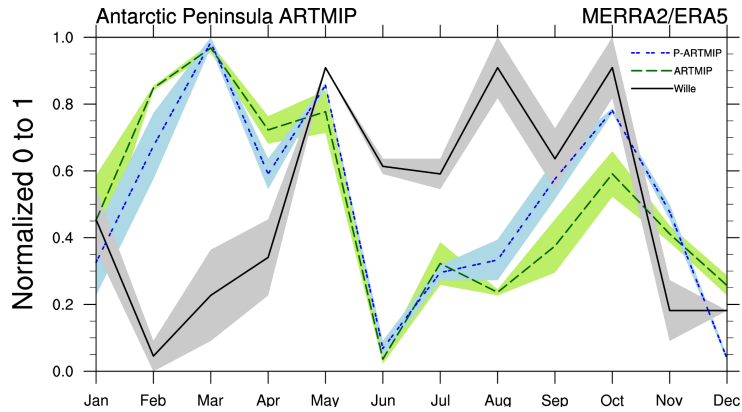
**Figure S2.** Modes of variability spatial patterns and timeseries for SAM (first row), PSA2 (second row), PDO (third row), IOD (fourth row). Nino3.4 timeseries is shown with IOD for reference.



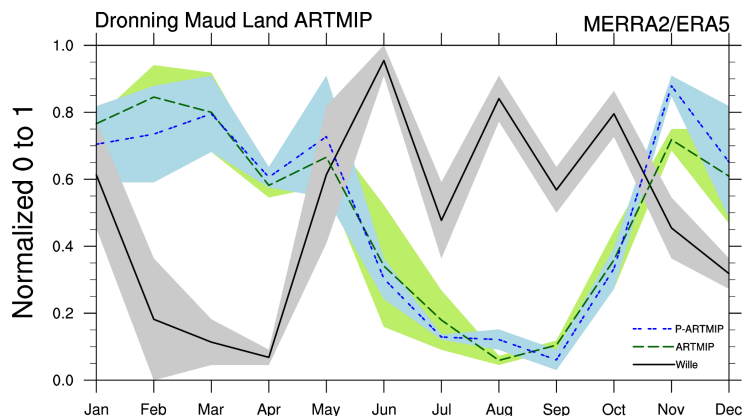
127  
 128  
 129  
 130  
 131  
 132  
 133  
 134  
 135  
 136  
 137

**Figure S3.** AR frequency ARTMIP Tier 1 and Tier 2 ARDTs (% time relative to analysis period) across longitudinal transect around the continent of Antarctica for all methods Tier 1 (MERRA2 1980-2016) (upper left), and individually, Tier 1 and participating Tier 2 (all other panels) where ERA5 analysis base period is 2000-2019. ARDTs with polar constraints (P-ARTMIP) are noted in individual panel titles. Wille ARDTs capture ARs consistently across all longitudes where most other ARDTs preferentially detect the Antarctic Peninsula.

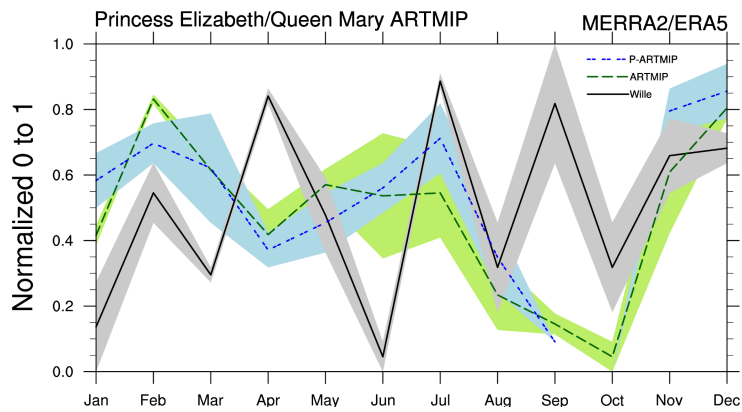
138



139



140



141

142 **Figure S4.** Same as Figure 2 in main text, except for regional locations around Antarctica,  
 143 Antarctic Peninsula (a), East Antarctica, Dronning Maud Land (b), and East Antarctica, Princess  
 144 Elizabeth and Queen Mary Land (c).

145

146

147

148

149

ARDT Name/Developer	Type	Algorithm Summary	DOI Reference
AR-Connect**	Global	Object identification; Absolute: IVT thresholds used = 700 kg/m/s for seeding, 300, for region growing; Time stitching, minimum 24-hour period; Global weighted centroid of AR event must be outside tropics (23.25 N - 23.25 S)	10.1029/2020JD033425
ClimateNet_DL**	Global	Deep learning based segmentation; Trained on ~500 expert labeled images; Threshold free; input fields are IWV, U850, V850, SLP; Time slice condition	10.5194/gmd-14-107-2021
Guan_Waliser_v2**	Global - Polar constraints	Length >2000km and length width ratio >2; Coherent IVT direction within 45° of AR shape orientation and with a poleward component; Relative: 85th percentile IVT; Absolute min requirement designed for polar locations: 100kg/m/s IVT; Time slice condition	10.1002/2015JD024257 10.1175/JHM-D-17-0114.1
Lora_v2**	Global - Polar constraints	Length >= 2000km; Relative/Absolute : IVT 225 kg/m/s above time/latitude dependent threshold using 30-day running mean and zonal average of IWV; Time slice condition	10.1016/j.epsl.2020.116293
Mundhenk_v3**	Global	>1400km length, aspect ratio 1:4, lat limit >16N/S, axis orientation based on IVT; Relative IVT percentiles and/or anomalies both temporal and spatial; Time slice condition	10.1175/JCLI-D-15-0655.1
PanLu	Global	1) Length>2000km; 2) Length-Width ratio>2; 3) sum of turning angle<360; 4) percentage within tropics < 95%; 5) 50% < percentage within tropics < 95% or percentage with IVT direction smaller than 15 degrees <50%; Two relative thresholds. Local threshold: smoothed 85% quantile IVT field using the Gaussian kernel density smoothing technique; regional threshold: the 80% quantile of IVT for all grids within 80N and 80S; Time stitching: last for at least 18 hours	10.1029/2018WR024407 10.1029/2020GL089477
Reid250	Global	Length > 2000km; Length-Width ratio > 2; orientation angle >10°; Absolute. IVT > 250 kg/m/s; IVT > 500 kg/m/s; Time slice condition	10.1029/2020JD032897
Rutz	Global	Length >= 2000km; Absolute: IVT (surface to 100mb) = 250kg/m/s; Time slice	10.1175/MWR-D-13-00168.1



		condition; low value on tropics	
SAIL_v1	Global - Polar constraints	Length $\geq 250$ km; Length-to-width $\geq 5$ ; Length is estimated along the "ridge" taking IVT into account; Width is the median of widths estimated in each point of AR ridge; Relative: IVT-IVT_RM $> 100$ kg/m/s. IVT_RM is climatological IVT running mean with 20-day windows; Time slice condition	Experimental
Teca_Bard_v1	Global	Runs 1,024 AR detectors simultaneously. Percentile threshold, minimum area, and filter latitude width are all sampled from a posterior distribution that is designed to optimize global AR counts relative to a dataset of AR counts from a set of experts.; Relative threshold (based on spatial percentile for each timestep); An inverted Gaussian filter is applied at the equator to damp out the ITCZ; Time slice condition	10.5194/gmd-13-6131-2020
TEMPEST (IVT threshold 250)	Global	Contains both an absolute threshold (typically set at IVT $>250$ kg/m/s) and a relative threshold (which uses a local Laplacian of IVT, typically set at $\text{del}^2$ IVT $< -50$ k); Laplacian IVT thresholds most effective for widths $>1000$ km; cluster size minimum = 120000km <sup>2</sup> ; Time stitching condition, Global, but latitude $\geq 15^\circ$	10.5194/gmd-10-1069-2017
Wille_IWV	Antarctic Specific	Length $> 20^\circ$ (2000 km) equatorward with no breaks; Defined as AR landfall if AR shape overlaps a land grid cell; Relative $> 98$ th percentile IWV based on monthly climatological means; Time slice condition	10.1038/s41561-019-0460-1 10.1029/2020JD033788
Wille_vIVT**	Antarctic Specific	Length $> 20^\circ$ (2000 km) equatorward with no breaks; Defined as AR landfall if AR shape overlaps a land grid cell; Relative $> 98$ th percentile vIVT based on monthly climatological means; Time slice condition	10.1038/s41561-019-0460-1 10.1029/2020JD033788

150

151 **Supplemental Table S1.** ARTMIP ARDTs and references are listed. 13 Tier 1 (MERRA2) and  
 152 6 Tier 2 (ERA5) ARDTs are included in this study. Selection was determined by including any  
 153 catalogue that captured ARs over Antarctica. Regression and MOV analysis was only performed  
 154 on ARDTs with polar constraints (5 ARDTs) to minimize error by only applying ARDTs fit for  
 155 purpose. \*\*ARDTs have both Tier 1 (MERRA2) and Tier 2 (ERA5) catalogue entries.

156 Algorithm summaries are also available on the ARTMIP webpage

157 (<https://www.cgd.ucar.edu/projects/artmip/algorithms.html>)

158

159

160

161  
162  
163  
164  
165  
166  
167  
168  
169  
170  
171  
172  
173  
174  
175  
176  
177  
178  
179  
180  
181  
182  
183  
184  
185  
186  
187  
188  
189  
190  
191  
192  
193  
194  
195  
196  
197  
198  
199  
200  
201  
202  
203  
204  
205  
206

## References for Supplemental

- Guan, B., and D. E. Waliser, (2015). Detection of atmospheric rivers: evaluation and application of an algorithm for global studies. *J. Geophys. Res. Atmos.*, 120, 12, 514–535.
- Kashinath, K., Mudigonda, M., Kim, S., Kapp-Schwoerer, L., Graubner, A., Karaismailoglu, E., Von Kleist, L., Kurth, T., Greiner, A., Mahesh, A. and Yang, K., (2021). ClimateNet: an expert-labeled open dataset and deep learning architecture for enabling high-precision analyses of extreme weather. *Geoscientific Model Development*, 14(1), pp.107-124.
- Mundhenk, B. D., E. A. Barnes, and E. D. Maloney (2016). All-season climatology and variability of atmospheric river frequencies over the North Pacific, *J. Climate*, 29, 4885–4903.
- O’Brien, T. A., Risser, M. D., Loring, B., Elbashandy, A. A., Krishnan, H., Johnson, J., Patricola, C. M., O’Brien, J. P., Mahesh, A., Arriaga Ramirez, S., Rhoades, A. M., Charn, A., Inda Díaz, H., & Collins, W. D. (2020). Detection of atmospheric rivers with inline uncertainty quantification: TECA-BARD v1.0.1. *Geoscientific Model Development*, 13(12), 6131–6148.
- Pan, M. and Lu, M. (2019). A Novel Atmospheric River Identification Algorithm, *Water Resources Research*, 2019, 55: 6069-6087.
- Reid, K. J., King, A. D., Lane, T. P., & Short, E. (2020). The sensitivity of atmospheric river identification to integrated water vapor transport threshold, resolution, and regridding method. *Journal of Geophysical Research: Atmospheres*, 125, e2020JD032897.
- Rutz, J. J., W. J. Steenburgh, and F. M. Ralph, (2014). Climatological characteristics of atmospheric rivers and their inland penetration over the western United States. *Mon. Wea. Rev.*, 142, 905–920.
- Shearer, E. J., Nguyen, P., Sellars, S. L., Analui, B., Kawzenuk, B., Hsu, K., et al. (2020). Examination of global midlatitude atmospheric river lifecycles using an object-oriented methodology. *Journal of Geophysical Research: Atmospheres*, 125, e2020JD033425.
- Shields, C. A., Rutz, J. J., Leung, L.-Y., Ralph, F. M., Wehner, M., Kawzenuk, B., Lora, J. M., McClenny, E., Osborne, T., Payne, A. E., Ullrich, P., Gershunov, A., Goldenson, N., Guan, B., Qian, Y., Ramos, A. M., Sarangi, C., Sellars, S., Gorodetskaya, I., Kashinath, K., Kurlin, V., Mahoney, K., Muszynski, G., Pierce, R., Subramanian, A. C., Tome, R., Waliser, D., Walton, D., Wick, G., Wilson, A., Lavers, D., Prabhat, Collow, A., Krishnan, H., Magnusdottir, G., and Nguyen, P. (2018). Atmospheric River Tracking Method Intercomparison Project (ARTMIP): project goals and experimental design, *Geosci. Model Dev.*, 11, 2455-2474, <https://doi.org/10.5194/gmd-11-2455-2018>, 2018.

- 207 Skinner, C.B., Lora, J.M. Payne, A. E., Pouslen, C. J., (2020), Atmospheric river changes shaped  
208 mid-latitude hydroclimate since the mid-Holocene, *Earth and Planetary Science Letters*, 541.  
209
- 210 Ullrich, P.A. and Zarzycki, C.M., (2017). TempestExtremes: A framework for scale-insensitive  
211 pointwise feature tracking on unstructured grids. *Geoscientific Model Development*, 10(3),  
212 pp.1069-1090.  
213
- 214 Wille, J.D., Favier, V., Dufour, A. et al. (2019). West Antarctic surface melt triggered by  
215 atmospheric rivers. *Nat. Geosci.* 12, 911–916. <https://doi.org/10.1038/s41561-019-0460-1>  
216
- 217 Wille, J. D., Favier, V., Gorodetskaya, I. V., Agosta, C., Kittel, C., Beeman, J. C., et al. (2021).  
218 Antarctic atmospheric river climatology and precipitation impacts. *Journal of Geophysical*  
219 *Research: Atmospheres*, 126, e2020JD033788.